Three-Dimensional Magnetic Field Measurements in a Single SERF Atomic-Magnetometer Cell

Alexander Gusarov[1], David Levron[2], Eugene Paperno[1], Reuben Shuker[2], and Andrei Ben-Amar Baranga[2,3]

[1]Department of Electrical and Computer Engineering, Ben-Gurion University of the Negev, 84105 Beer-Sheva, Israel
[2]Department of Physics, Ben-Gurion University of the Negev, 84105 Beer-Sheva, Israel
[3]Department of Physics, Nuclear Research Center-Negev, 84190 Beer-Sheva, Israel

We show that a single-cell spin-exchange relaxation-free (SERF) atomic magnetometer can be used for 3-D field measurements. The 3-D operation is achieved by optically pumping the magnetometer cell in successive layers perpendicular to the laser probe beam and by collecting the signals with a photodiode array. The vapor cell is thus divided into voxels acting as local atomic magnetometers. Each voxel's contribution to the probe linear polarization rotation is proportional to the convolution of the local polarization and the magnetic field. The layers are pumped in sequence without waiting for the atomic polarization in the previously pumped layer to relax to zero, consequently, reducing the total measurement time. The photodiode signals are the sum of accumulated linear polarization rotation caused by all the layers. These signals are processed by a deconvolution algorithm that extracts the information originating from each individual voxel. Our theoretical analysis and experimental results show that the time of a single-layer pumping can be reduced below the atomic-cell relaxation time constant, with almost no loss of precision.

Index Terms—Atomic magnetometer, magnetoencephallography (MEG), spin-exchange relaxation-free (SERF), 3-D measurements.

I. INTRODUCTION

MEASURING very low magnetic fields is of major importance in various scientific fields such as biology, geology, neurology, low-field nuclear magnetic resonance (NMR), nondestructive testing (NDT), etc. In many cases the end result is the localization of magnetic field sources. For example, magnetoencephalography (MEG) requires measurements at multiple sites to provide enough data for the localization of a large number of magnetic sources within the brain. If a dynamic magnetic source is monitored, fast data acquisition is necessary.

In the last decades, very low magnetic field measurements, in general, and biomagnetic monitoring, in particular, were performed only by cryogenic, low-T_c superconducting quantum interference device magnetometers (SQUIDs). Such liquid He devices impose strict mechanical requirements with a very high apparatus and operational cost. Recently, optical or atomic magnetometers have attracted increasing attention as they get smaller in volume and higher in sensitivity, competing successfully with SQUID's (see [1] and references therein).

An atomic magnetometer is based on measuring the Larmor frequency of an atomic spin in an external magnetic field. As shown in Fig. 1, the spins of the atoms are oriented by optical pumping along an incoming circularly polarized laser beam, which is tuned to a specific atomic transition. A magnetic field perpendicular to the pumping beam rotates the spins by an angle α which is proportional to the magnetic field intensity. A linearly polarized probe beam, perpendicular to both the pump beam and the magnetic field, measures the angle α of the spin rotation and, hence, the absolute intensity of the magnetic field. This is obtained by monitoring the rotation of the probe beam
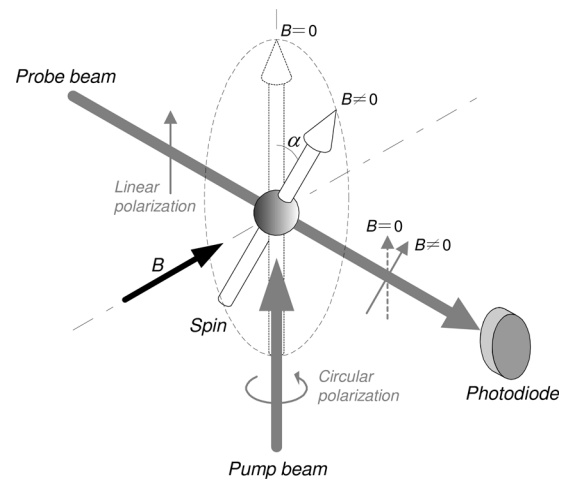
Fig. 1. Operating principle of an atomic magnetometer.

polarization plane, an effect known as resonant Faraday rotation. To avoid absorption, the probe beam wavelength is detuned from the resonant absorption wavelength of the atomic transition.

In principle, a single atom can serve as a magnetic field detector. However, a viable detector should incorporate a large number of aligned atoms to provide a high enough signal-to-noise ratio (SNR). A very good example of such a device is the spin-exchange relaxation-free (SERF) magnetometer characterized by high-density atomic vapor, efficient magnetic shielding (>1000), and high-pressure buffer gas (>1 atm) [2]–[4]. For a 1-cm^3 measurement volume in an alkali metal vapor cell, the SERF magnetometer sensitivity threshold is better than 0.5 fT/$\sqrt{\text{Hz}}$ [4]. The SERF magnetometer has already demonstrated the capability of 2-D multichannel operation (see Fig. 2) [6]–[8].

We show in this paper that a single-cell SERF magnetometer can be used for 3-D field measurements. The 3-D operation is achieved by repetitively pumping the magnetometer cell in successive layers perpendicular to the probe beam (see Fig. 3) and
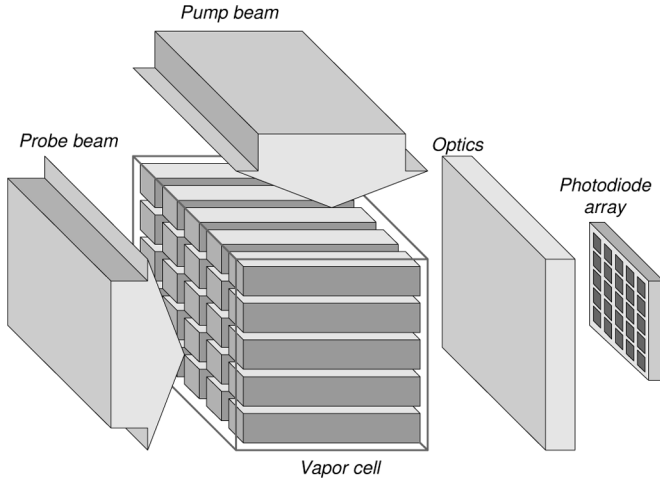
Fig. 2. Two-dimensional operation of a single SERF magnetometer cell.
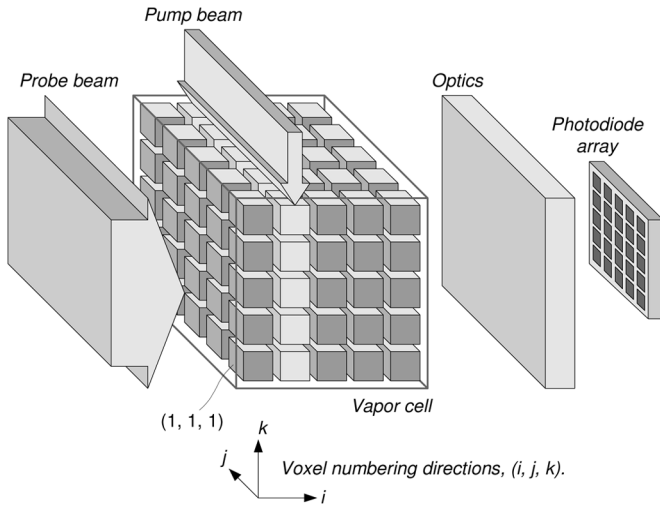
Fig. 3. Three-dimensional operation of a single SERF magnetometer cell. The pump beam is sequentially illuminating consecutive layers in the vapor cell.

processing the signals, detected with the photodiode array, by a special algorithm that extracts the information originating from each individual layer.

II. METHOD

A. Theory

Fig. 3 shows the geometrical arrangement of the scanning process. The pump beam illuminates the vapor cell layer by layer, going from the first $(i = 1)$ layer to the last $(i = 5)$ layer and then restarting again from the first. The pump intensity is kept constant for a dwell time Δt. The signal obtained from measuring the polarization rotation of the probe beam is recorded as a function of time. The polarization in each layer is building up when the layer illuminated and is decaying when the layer is "in the dark."

The probe beam illuminates the entire cell. Each element in the photodiode array defines a "pencil" of vapor, and each layer defines a voxel in each pencil. The time evolution of the polarization of the vapor atoms in each voxel is described by the

Bloch equation [9]. Due to the high pressure of the buffer gas, we neglect the diffusion term in this equation.

The "nuclear slowing factor," which changes the precession rate of the spins around the direction of the magnetic field, is given by [4]

$$q(P) = \frac{2 + 4\cosh(\beta)}{\cosh(\beta)} \text{ with } P = \tanh\left(\frac{\beta}{2}\right). \tag{1}$$

The factor $q(P)$ for potassium atoms, used in our SERF magnetometer, varies from 6 to 4 for $P = 0$ to $P = 1$, correspondingly. To linearize the Bloch equation, we choose the mean value of q as the constant for our calculations.

The buildup of the polarization in the pump beam direction is given by

$$P_{\text{rise}}(t) = \frac{sR}{R + \sum \Gamma}\left[1 - \exp\left(-\frac{R + \sum \Gamma}{q}t\right)\right] \tag{2}$$

where s represents the degree of circular polarization of the pump beam, R is the optical pumping rate, $\sum \Gamma$ is the sum of all the spin destruction rates (K-He collisions, probe beam contribution, etc.), and t is the elapsed time from the onset of the pump beam in the corresponding layer.

The decay of the atomic polarization, once the pump beam is turned off (shifted to the next layer), is approximately given by

$$P_{\text{fall}}(t) = P_0 \exp\left(-\frac{\sum \Gamma}{q}t\right) = P_0 \exp\left(-\frac{t}{T}\right) \tag{3}$$

where t here is measured from the moment the pump beam in the layer was turned off, and P_0 is the polarization at *that* time. The atomic decay time of the polarization, T, is defined in (3). Definitions of the optical pumping rate and all the other variables are given in [4] and [9].

B. Algorithm for Minimizing the Measurement Time

From [9], each layer's contribution to the probe polarization rotation is proportional to the product of the magnetic field in the j-direction in Fig. 3 and the atomic polarization of the layer. Isolation of the contribution of each layer to the polarization plane rotation of the probe beam requires waiting for the atomic polarization in the previously pumped layer to relax to zero. Residual atomic polarization would cause the photodiode signal to be the sum of accumulated polarization rotation caused by all the layers. Waiting for the polarization to relax would make the measurement time prohibitively long.

To decrease the measurement time, we suggest pumping consecutive layers with no waiting time and analyzing the measured signal by the following algorithm. The expected signal from n layers, each exposed to a different magnetic field $B_i(t)$, assumed spatially uniform in the voxel, can be described as

$$\text{Signal} = \sum_1^n \int_0^{n\Delta t} P_i(t - \tau_i)B_i(t)dt \tag{4}$$

where $\tau_i = (i - 1)\Delta t$ is the time of the onset of the illumination of the ith layer, P_i is given by (2) for a buildup stage and by (3) for a decay stage. For example, when the fifth layer is illuminated $(4\Delta t < t < 5\Delta t)$, $\tau_1 = 0, \tau_2 = \Delta t, \tau_3 = 2\Delta t, \tau_4 =$
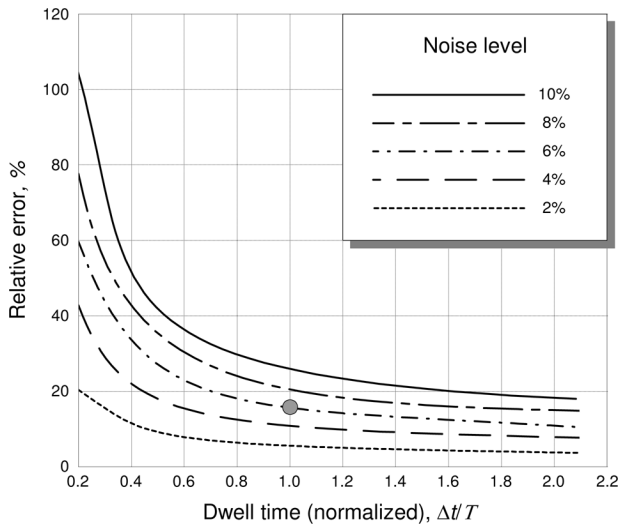
Fig. 4. Relative error in measuring B_i versus normalized dwell time for a five-layer cell. The decay time constant, T, is 190 ms, and the buildup time for the polarization, $1/(R + \Sigma\Gamma)$, is 30 ms. The gray dot corresponds to the experimental results, where the measurement noise is 6%, $\Delta t/T \approx 1$, and the relative measurement (deconvolution) error is about 15%.

Fig. 5. Experimental setup.

$3\Delta t$, and $\tau_5 = 4\Delta t$, whereas P_1, P_2, P_3, and P_4 have the functional form (3), and P_5 has the form (2).

The signal (4) is actually a sum of convolutions of the polarization and the magnetic field. Extracting the information corresponding to the magnetic fields from the signal (4) can be achieved by deconvolution.

To investigate the deconvolution precision as a function of the measurement noise, we have performed numerical simulations with temporally constant field values for each layer. The physical parameters in (2) and (3) are measured in our experimental system and given in the caption of Fig. 4. A Gaussian white noise is added to the atomic polarization values in (2) and (3). The noise levels relative to the maximum atomic polarization value were chosen between 2 and 10%. The signal (4) bandwidth was set at 100 Hz. Fig. 4 presents the simulation results. From this figure, we can deduce that the time of a single-layer pumping can be reduced down to $0.8T$ with almost no loss of precision.

We have also simulated the case of sinusoidally varying magnetic fields. These simulations show that the relative systematic error in such measurements goes down to 1% for magnetic field frequency in the range from $0.1/T$ to $5/T$. For $T = 50$ ms, this frequency range corresponds to 2 to 100 Hz.

III. EXPERIMENT

Fig. 5 depicts the experimental setup. Two external-cavity diode lasers (ECDLs) where used as the pump and probe beams. These two ECDLs are stabilized and frequency controlled by gratings with 1800 grooves/mm in a Littrow configuration [10]. The lasers are tuned to either the resonance wavelength of the D1 potassium for the pump beam, or to the desired detuning from resonance for the probe beam. Their line-widths are 0.1 nm at half maximum. The linear polarization of the probe beam is modulated by a Faraday modulator. The modulation frequency is 3 kHz, and the amplitude of the rotation angle is about $3°$.
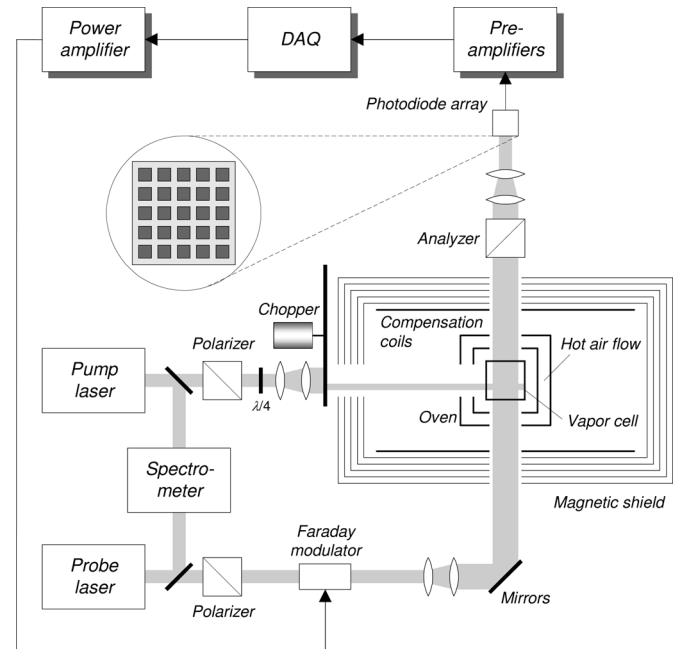
A cubic potassium cell (3 cm on the side) is mounted inside an oven. The cell contains 2.5 amagat of ^{4}He, 50 torr N_2, and a drop of metal K. The cell is heated by hot air flow, and its temperature is regulated by a thermocontroller using a thermocouple attached to the cell. The operating temperature is 170–200 °C. The oven and the cell are situated inside a five-layer magnetic shield with a shielding coefficient of about 10^4, essential to SERF operation [4]. The sensitivity threshold of the system for a 2-cm^3 volume is 20 fT/$\sqrt{\text{Hz}}$. The sequential pumping of consecutive layers in the cell is achieved by a specially designed optical chopper.

The data acquisition system (DAQ) consists of a Hamamatsu 5×5 photodiode array connected to the preamplifier board and an array of analog-to-digital converters the output of which is accumulated in a computer. The signal is digitally filtered by digital lock-in amplifiers to produce up to 25 independent measurement channels of the magnetic field. The voxel size is 2 mm $\times$ 2 mm $\times$ 3 mm, and its sensitivity threshold is about 500 fT/$\sqrt{\text{Hz}}$.

To demonstrate the applicability of the suggested method, we show in Fig. 6 the information obtained from three consecutive layers. The black line in Fig. 6 shows the raw data, and the thin gray lines denote the extreme limits of the signal reconstruction. The measurement noise is 6%, $\Delta t/T \approx 1$, and the relative measurement (deconvolution) error is about 15% which is in a good agreement with the theoretical results (see Fig. 4).

IV. CONCLUSION

A novel method for the 3-D operation of the SERF atomic magnetometer is suggested. The method is based on pumping the magnetometer cell in successive layers perpendicular to the probe beam and processing the signals, detected with the photodiode array, by a deconvolution algorithm that extracts the information originated from each individual layer.
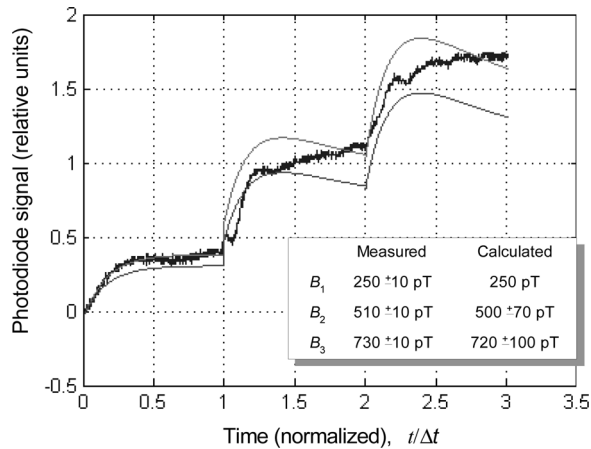
Fig. 6. Single-channel signal with three sequential layers pumping. The magnetic field "calculated" for each voxel is found by the deconvolution. The "measured" magnetic field has been separately measured in the conventional SERF mode of constant pumping. For calibration, we take B_1 (calculated) $\equiv$ B_1 (measured). The black line represents the measured signal, and the thin gray lines denote the extreme limits of the signal reconstruction.

It has been shown theoretically for the case of dc magnetic field measurements that the deconvolution allows us to decrease the time of a single-layer pumping down to $0.8T$, with almost no loss of precision. It has also been shown that in the case of sinusoidally varying magnetic fields the relative systematic error of the dc component goes down to 2%, provided that the magnetic field frequency is in the range from $5/T$ to $10/T$. For $T = 100$ ms, this frequency range corresponds to 50–100 Hz.

The applicability of the method has been tested experimentally. A good agreement between the theoretical and experimental data has been obtained.

References

[1] D. Budker and M. Romalis, "Optical magnetometry," *Nature Phys.*, vol. 3, pp. 227–234, Apr. 2007.
[2] W. Happer and H. Tang, "Spin-exchange shift and narrowing of magnetic resonance lines in optically pumped alkali vapors," *Phys. Rev. Lett.*, vol. 31, pp. 273–276, Jul. 1973.
[3] W. Happer and A. C. Tam, "Effect of rapid spin exchange on the magnetic-resonance spectrum of alkali vapors," *Phys. Rev. A*, vol. 16, pp. 1877–1891, Nov. 1977.
[4] J. C. Allred, R. N. Lyman, T. W. Kornak, and M. V. Romalis, "High-sensitivity atomic magnetometer unaffected by spin-exchange relaxation," *Phys. Rev. Lett.*, vol. 89, pp. 130801-1–130801-4, Sep. 2002.
[5] I. K. Kominis, T. W. Kornack, J. C. Allred, and M. V. Romalis, "A subfemptotesla multichannel atomic magnetometer," *Nature*, vol. 422, pp. 596–599, Apr. 2003.
[6] A. Ben-Amar Baranga, D. Hoffman, H. Xia, and M. V. Romalis, "An atomic magnetometer for brain activity imaging," in *Proc. 14th IEEE-NPSS Real Time Conf. 2005 (RT2005)*, pp. 3–4.
[7] H. Xia, A. Ben-Amar Baranga, D. Hoffman, and M. V. Romalis, "Magnetoencephalography with an atomic magnetometer," *Appl. Phys. Lett.*, vol. 89, pp. 211104-1–211104-3, Nov. 2006.
[8] A. Ben-Amar Baranga, S. Appelt, C. J. Erickson, A. R. Young, and W. Happer, "Alkali-metal-atom polarization imaging in high-pressure optical-pumping cells," *Phys. Rev. A*, pp. 2282–2294, Sep. 1998.
[9] M. P. Ledbetter, I. M. Savukov, V. M. Acosta, D. Budker, and M. V. Romalis, "Spin-exchange relaxation free magnetometry with Cs vapor," *Phys. Rev. A*, vol. 77, pp. 033408-1–033408-7, Mar. 2008.
[10] A. S. Arnold, J. S. Wilson, and M. G. Bosier, "A simple extended-cavity diode laser," *Rev. Sci. Instrum.*, vol. 69, pp. 1236–1239, Mar. 1998.